Symmetry in mesoscale circulations explains weak impact of trade cumulus self-organisation on the radiation budget in large-eddy simulations

M. Janssens[1,2], F. Jansson[2], P. Alinaghi[2], F. Glassmeier[2], A. P. Siebesma[2,3]

[1]Wageningen University & Research, Wageningen, The Netherlands
[2]Delft University of Technology, Delft, The Netherlands
[3]Royal Netherlands Meteorological Institute, De Bilt, The Netherlands

Key Points:

- Simulated shallow cumulus convection spontaneously grows into mesoscale structures across a climatological range of idealised environments
- Letting the convection self-organise gives a systematic 0.5 $\mathrm{Wm^{-2}}$ top-of-atmosphere radiative cooling, due to small offsetting effects
- Mesoscale circulations weakly alter the shortwave cloud-radiative effect because their ascent and descent symmetrically modify cloudiness

*

Corresponding author: Martin Janssens, `martin.janssens@wur.nl`

Abstract

We investigate if mesoscale self-organisation of trade cumuli in 150 km-domain large-eddy simulations modifies the top-of-atmosphere radiation budget relative to 10 km-domain simulations, across 77 characteristic, idealised environments. In large domains, self-generated mesoscale circulations produce fewer, larger and deeper clouds, raising the cloud albedo. Yet they also precipitate more than small-domain cumuli, drying and warming the cloud layer, and reducing the cloud cover. Consequently, the large-domains' shortwave cloud-radiative effect's cooling weakly reduces, and their clear-sky outgoing longwave radiation's cooling weakly increases, for a net cooling (-0.5 W m^{-2}). This cooling is generally smaller than the large-domain radiation's sensitivity to large-scale meteorological variability, which is similar in small-domain simulations and observations. Hence, spontaneously developing mesoscale circulations do not alter weak trade-cumulus feedback estimates from small domains. We explain this with a symmetry hypothesis: ascending and descending branches of mesoscale circulations symmetrically increase and reduce cloudiness, weakly modifying the mean radiation budget.

Plain Language Summary

Fields of shallow cumulus clouds over the tropical oceans cool our climate. How much cooling they give with global warming is a long-standing, leading uncertainty in climate projection. Detailed process models estimate this cooling to be resilient to warming-related modifications of the large-scale tropical environment. Yet these models were usually run in small (10 km) domains, while real-world cumuli often grow beyond 100 km in width. Therefore, we compare the cooling in 10 km and 150 km-sized detailed process models. Over a large range of idealised environments, the 150 km-domain simulations spontaneously develop large cloud structures, which cannot live in 10 km domains. However, the circulations associated with these large clouds simultaneously reduce cloudiness elsewhere, giving small changes in the overall cloudiness, and cooling. Hence, although they produce cloud patterns more reminiscent of the real world, our large-domain simulations predict a similar resilience to changes in the tropical environment, and thus to warming, as small domains and observations.

1 Introduction

Uncertainties in how trade cumuli respond to warming have long shaped the uncertainty margins in climate model-estimates of Earth's climate sensitivity (e.g. Bony & Dufresne, 2005; Vial et al., 2013; Zelinka et al., 2020). Significant progress has still been made in constraining the trade-cumulus feedback on warming in recent years, by observing how trade cumuli vary in today's climate at the daily (Vial et al., 2023), seasonal (Brueck et al., 2015) and inter-annual (Myers & Norris, 2016; Cesana et al., 2019; Scott et al., 2020) time scale. By observing which large-scale ($>$ 500 km) "cloud controlling factors" (CCFs, Klein et al., 2017) are responsible for variations in cloudiness in today's world, and combining such sensitivities with estimates of how the CCFs will change with warming, a weak trade-cumulus feedback ($<$ 0.1 W m^{-2} K^{-1}) emerges as the most likely outcome (Sherwood et al., 2020; Cesana & Del Genio, 2021; Ceppi & Nowack, 2021; Myers et al., 2021).

Such assessments are complemented by process-understanding from large-eddy simulations (LESs) (Sherwood et al., 2020), traditionally run on small ($O(10)$ km) domains. These LESs too project a weak trade-cumulus feedback on idealised tropical warming (Blossey et al., 2013; Bretherton et al., 2013; Bretherton, 2015; Tan et al., 2017; Radtke et al., 2021). Yet recent observations highlight that within a 10-500 km ("mesoscale") cloud field, there are large co-variations in cloudiness and vertical motion (George et al., 2021; Vogel et al., 2022), courtesy of mesoscale circulations (George et al., 2023). Equivalently, several LES case studies on 50 km-scale domains and beyond suggest that the convection will "self-organise" into a different regime than in identical small-domain setups (e.g. Seifert & Heus, 2013; Vogel et al., 2016; Bretherton & Blossey, 2017; Alinaghi et al., 2024), through feedbacks between mesoscale circulations and convection. How can observations, which measure the radiation from nature's actual mesoscale cloud patterns, and small-domain LES, which excludes mesoscale self-organisation by definition, then both predict a weak trade cumulus feedback?

To help answer that, we here compare the top-of-atmosphere (TOA) radiation balance between LESs in domains with and without mesoscales. Specifically, we study the Cloud Botany ensemble (Jansson et al., 2023), where we control the initial environment and boundary forcing of 150- and 10-km doubly periodic domains with i.a. five parameters that embody salient CCFs of observational studies: i) sea surface liquid water potential temperature θ_{l_s}, varied together with vertically constant θ_l offsets throughout the troposphere, ii) near-surface (10 m) geostrophic wind speed U, iii) free-tropospheric lapse rate of θ_l, Γ_{θ_l}, iv) total water specific humidity q_t's free tropospheric scale height (h_{q_t}), and v) domain-averaged, cloud-layer subsidence velocity w_{ls}. We vary these CCFs individually and together, giving 103 simulations spanning the climatological envelope of today's trades.

2 Self-organised mesoscale cloud patterns are ubiquitous across trade-wind environments

In the following, we focus on the 77/103 simulations which return cloudy solutions, and run $\geq$60 h. To visualise mesoscale cloud patterns in these simulations, we follow Janssens et al. (2021): For all cloud fields between 6-60 h after initialisation at a 5 min interval, we calculate ten "organisation metrics" of the spatial patterning of the clouds. We standardise these metrics over time and simulation, and project the resulting data set onto its principal components (PCs). The two first PCs explain 82% of all ten metrics' variance across the ensemble. We therefore treat these PCs as effective organisation metrics.

The PCs describe similar pattern characteristics as the satellite images studied by Janssens et al. (2021), though the simulated cloud fields are both smaller (150 km vs. 500 km) and forced by a less heterogeneous set of processes. The first PC portrays a typical cloud length scale (Spec. length, Mean cloud object length $\bar{l}$); the second PC captures the complementary length scale of cloud-free regions (cloud cover f, Open sky). Accordingly, we name these components L_c and L_o.

Figure 1 a) shows examples of cloud fields on the plane spanned by L_c and L_o, revealing a broad variety of cloud patterns in the simulations. They include fields of small, uniformly distributed cumuli (left), aggregates of such cumuli in clusters and bands of various sizes (centre, centre-top), and large, bright clusters and squalls with similarly scaled cloud-free regions, themselves lined by bright clouds (right, similar to e.g. Seifert & Heus, 2013; Vogel et al., 2016; Lamaakel & Matheou, 2022). These large structures also often possess optically thin cloud sheets, resembling the stratiform clouds found atop precipitating shallow convection both in simulations (Vogel et al., 2019; Dauhut et al., 2023) and nature (O et al., 2018; Wood et al., 2018).

Since all simulations are initialised in a spatially homogeneous atmosphere and driven by horizontally homogeneous forcing, all mesoscale cloud patterns are self-organised by convection-mesoscale dynamics feedbacks. The time series in fig. 1 c-e show that every simulation in the ensemble develops such patterns through increasing L_c, and slightly reducing L_o. That is, shallow convection spontaneously grows into mesoscale structures across the envelope of environments that is characteristic of the trades.

The growth in L_c is modulated by an oscillation in both L_c and L_o that follows the diurnal cycle of shortwave radiation, indicated by line colours in fig. 1 b-e and dark-

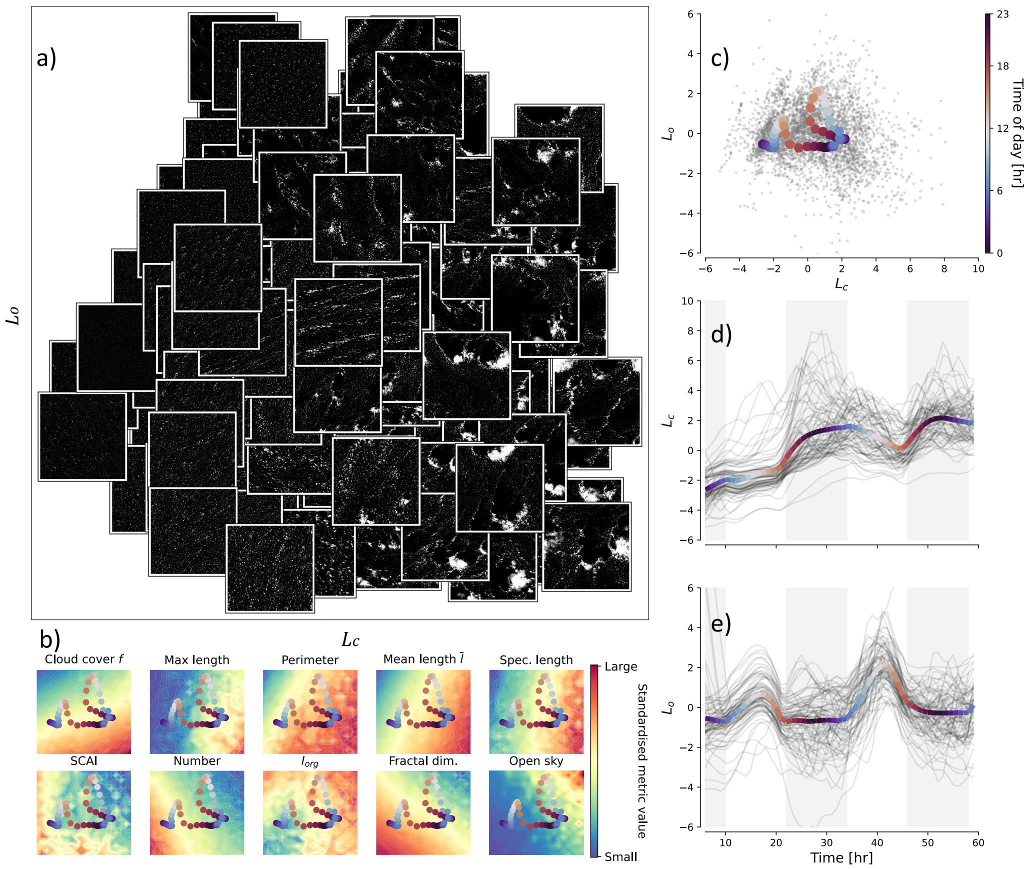

Figure 1. a) Cloud albedo in the plane-parallel approximation by Coakley and Chylek (1975), in example scenes, varying with L_c and L_o. b) Excerpts from a), coloured by standardised geometrical organisation metrics, and overlaid by ensemble-mean time evolution, coloured by time of day, see c). The time-evolution of L_c (d) and L_o (e) in all ensemble members is shown between 6-60 h after initialisation, also overlaid by the time-of-day-coloured ensemble-mean. Darkened background shading indicates night.

ened backgrounds in fig. 1 d and e. This cycle echoes the diurnal evolution of observed trade cumulus patterns (Vial et al., 2021), and is further explored in Alinaghi et al. (2024). It almost repeats itself after the second simulated day, reflecting how our simulations approach, but do not fully reach, a steady state. We therefore analyse this second day, between 30-54 h.

3 Mesoscale circulations enhance rainfall, but marginally affect the top-of-atmosphere radiation budget

3.1 Rainfall, cloudiness and cloud albedo

To understand how the growth of L_c and L_o modifies the TOA radiation balance, we first investigate how it affects the vertical structure of the state variables that determine the clear- and all-sky radiative transfer: θ_l, q_t, f and cloud-albedo α_c.

In our 150-km domain simulations, the self-organisation primarily affects these quantities by producing an order of magnitude more surface precipitation P_s (0.025 mm h^{-1})

than 10 km-domain simulations (0.002 mm h^{-1}). These differences arise because the large domains spontaneously develop mesoscale circulations, which aggregate water vapour into preferentially convecting regions (Bretherton & Blossey, 2017; Narenpitak et al., 2021; Janssens et al., 2022). As a result, substantial total water path fluctuations I' develop: Averaged over 10×10 km^2 sub-domains, fig. 2 a) shows that with respect to the domain-mean at each hour in each 150 km simulation, $I' \sim$ 2-4 mm. As I' increases, so does the hourly 10 km P_s (orange line fig. 2 a), in a shallow analogy of the well-established relationship between I and P_s across the tropics (Bretherton et al., 2004; Nuijens et al., 2009; Radtke et al., 2023). In fact, more than 80% of the precipitation in the 150 km ensemble falls in sub-domains where $I' > 0$. The 10 km domain simulations cannot produce the mesoscale circulations and cold pools needed to create these mesoscale moisture fluctuations ($I' = 0$ by construction). Their low 10 km P_s are indicated by light-grey scatter in fig. 2 a).

Two effects of the additional precipitation modify the 150 km-domain simulations' mean thermodynamic structure. First, the precipitating mesoscale systems heat the upper regions of the large-domain cloud layer relative to small domains (fig. 2 b, d), in line with simple models and small-domain LES (Albrecht, 1993; Stevens & Seifert, 2008; Bretherton et al., 2013). A mesoscale, cloud-layer weak-temperature-gradient constraint (Bretherton & Blossey, 2017; Janssens et al., 2022, 2024) efficiently communicates this latent heating from the mesoscale systems across the 150 km domains, resulting in weaker, lower domain-wide inversions than in 10 km domains (y-ticks in fig. 2 b). Second, the larger precipitation fluxes in large domains sediment additional moisture from their cloud layers, reducing horizontally-averaged q_t (fig. 2 c, e). The combined warming and drying lowers the cloud-layer relative humidity by 6% in the large-domain ensemble, relative to the small-domain ensemble (fig. S1).

The drier, warmer large-domain cloud layers have a slightly lower f than small domains (fig. 2 f). The cumulative, height-wise contribution to f ($f(z)$) attributes this reduction to the upper cloud layer (from around 1000 m), where both the drying and stabilisation is felt, and to the lower inversion, where less additional clouds develop. Yet, the larger convective systems which develop in the moist regions of 150-km domains are structurally geometrically thicker, more adiabatic and more liquid-water laden than the smaller clouds in the 10-km domains (Plank, 1969; Stephens, 1978; Benner & Curry, 1998; Zhao & Di Girolamo, 2007; Feingold et al., 2017, see Text S1). Hence, the organised convection in large domains has a slightly larger α_c than the unorganised convection in smaller domains (Alinaghi et al., 2023), both at a given height, and over a deeper layer (fig. 2 g).

In all, compared to 10 km domains, mesoscale self-organisation in 150 km domains gives both larger cloud structures (larger L_c) with larger α_c, and larger cloud-free areas (larger L_o) and reductions in f. Put differently, mesoscale dynamics concentrate cloudiness in fewer, larger structures, which live at the expense of the many, smaller clouds (fig. S2).

3.2 Impact on top-of-atmosphere radiative fluxes

In each ensemble, we next evaluate the top-of-atmosphere net radiation

$$N = -F\uparrow_{s,c} - F_{l,c}^{\uparrow} + C_s + C_l, \quad (1)$$

decomposed into clear-sky net outgoing shortwave and longwave radiative fluxes ($-F_{s,c}^{\uparrow}$ and $-F_{l,c}^{\uparrow}$), and shortwave and longwave cloud-radiative effects (C_s and C_l). These horizontally averaged terms are constructed from column-wise all- and clear-sky radiative fluxes, evaluated at runtime by the LES's radiative transfer model (Iacono et al., 2008).

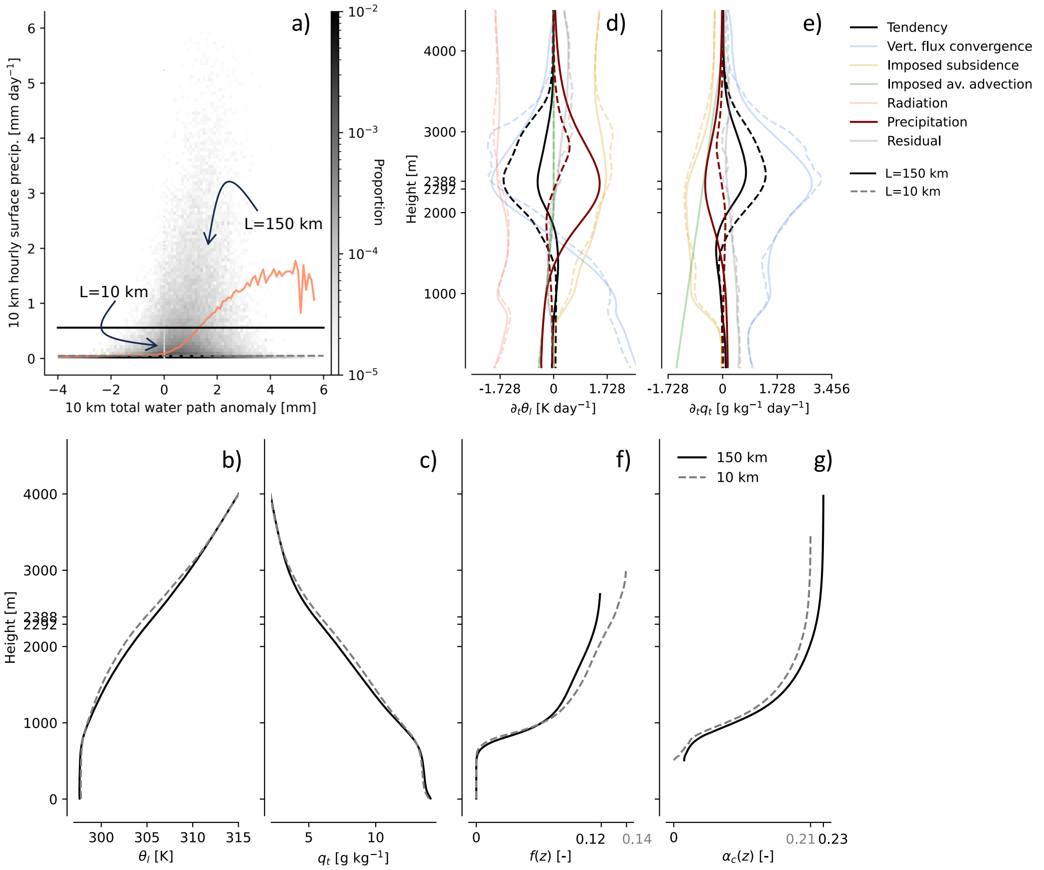

Figure 2. a): Joint histogram (shading) of the total water path fluctuation I' around the horizontal domain mean, and rain rate P_s, both averaged over 10×10 km^2 sub-domains and 1h, in all 150 km-domain simulations. The salmon line indicates the ensemble-mean P_s given I', light-grey scatter at $I' = 0$ indicates P_s in the 10 km-domain ensemble, and horizontal lines indicate the ensemble-mean P_s in 150-km domains (black, unbroken) and 10-km domains (grey, broken). b) and c): Ensemble-averaged θ_l and q_t profiles for 150 km-domain (black, unbroken) and 10 km-domain (grey, broken) simulations. d) and e): Terms contributing to horizontally averaged heating $\partial\theta_l/\partial t$ and moistening $\partial q_t/\partial t$, with the most different terms between ensembles - the tendency (black) and precipitation heating/drying (maroon) - emphasised. f) and g): cumulative contribution of model levels below z towards the cloud cover f at z ($f(z)$) and albedo in cloudy columns α_c at z ($\alpha_c(z)$), until the height where $f(z) = f$ and $\alpha_c(z) = \alpha_c$ (x-axis ticks). In figs. b-g, the results are averaged over 30-54 h.

Figure 3 a) plots the difference in each component between all 150 km and 10 km-domain simulations, i.e. $\Delta N = N_{150} - N_{10}$. It shows a small ensemble-averaged $\Delta N = -0.51$ W m^{-2}, arising from a small increase in clear-sky longwave cooling ($-\Delta F^{\uparrow}_{l,c} = -1.01$ W m^{-2}) and a reduction in C_l's warming ($\Delta C_l = -0.31$ W m^{-2}), which together offset a smaller cooling from C_s ($\Delta C_s = 0.82$ W m^{-2}).

The changes in all three terms can be understood in terms of the mean state's differences presented in fig. 2. First, writing $C_s = F^{\downarrow}_s f \alpha_c$, where $F^{\downarrow}_s$ is the TOA downwards shortwave radiative flux, we primarily attribute $\Delta C_s \approx F^{\downarrow}_s(\alpha_c \Delta f + f \Delta\alpha_c)$ to the reduction in f in 150 km domains, which outweigh the increases in α_c (fig. 3 b, left

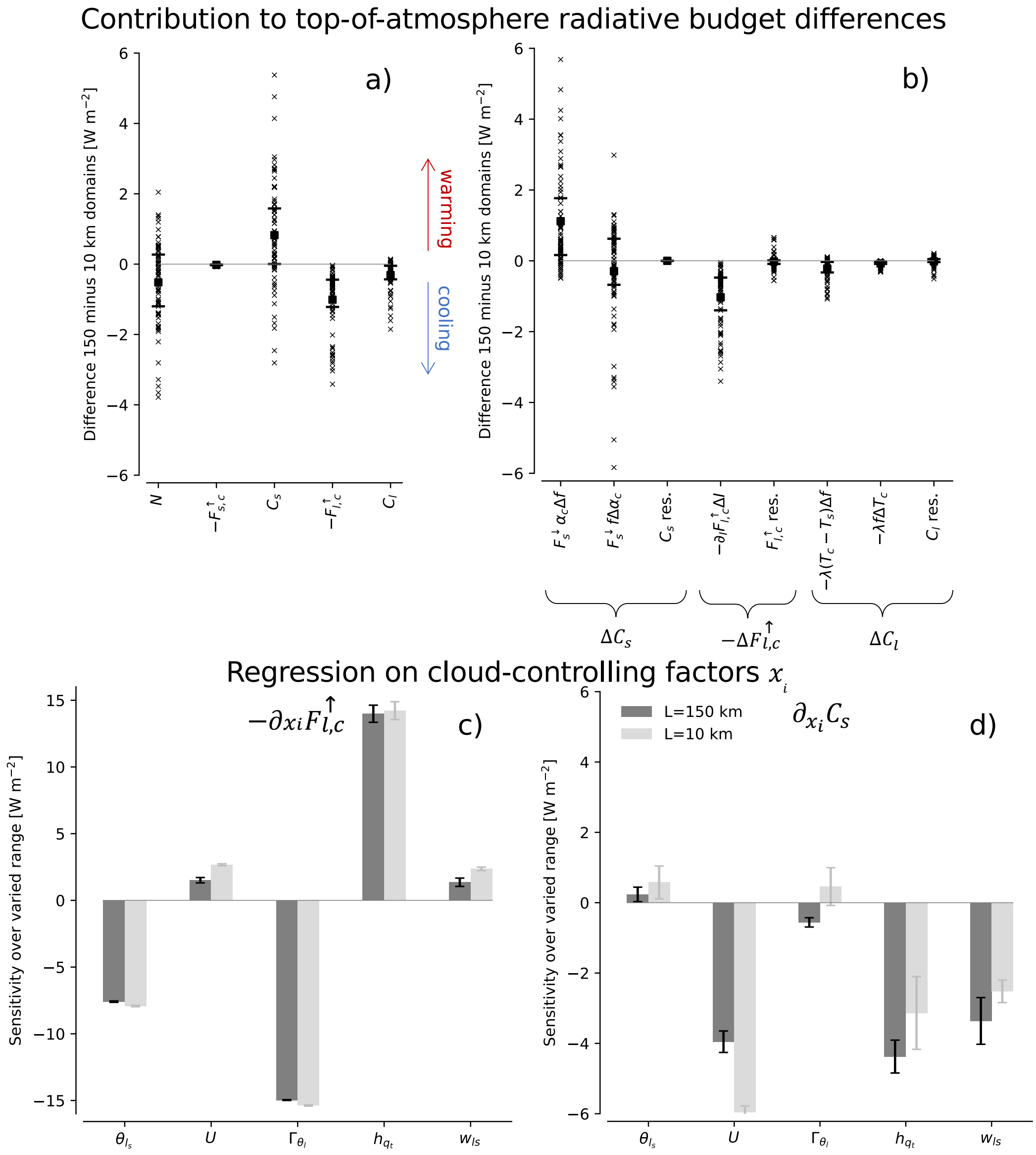

Figure 3. a): Differences in TOA net radiation between each 150 and 10 km domain simulation (ΔN, crosses) and its contributions from shortwave and longwave clear-sky fluxes ($-F_{s,c}^{\uparrow}$ and $-F_{l,c}^{\uparrow}$) and cloud-radiative effects (C_s and C_l). Circles and horizontal bars mark the mean and inter-quartile range over the ensemble members. b): As in a), with ΔC_s, $-\Delta F_{l,c}^{\uparrow}$ and ΔC_l broken down by the mean state changes in cloud cover f, cloud-albedo α_c, vertically integrated total water specific humidity I and cloud-layer temperature T_c (see text). Residuals in ΔC_s, $-\Delta F_{l,c}^{\uparrow}$ and ΔC_l when these contributions are summed are marked "res.". c) and d): Linear least-squares regression coefficients of C_s (c) and $F_{l,c}^{\uparrow}$ (d) on individual cloud-controlling factors, in large (dark) and small (light) domains. All variables are averaged between 30-54 h.

bracket). Second, modelling $C_l \approx -f\lambda_p(T_c - T_s)$ (e.g. McKim et al., 2024), with T_c and T_s the average cloud-layer and surface temperatures, and λ_p an appropriate longwave clear-sky feedback, $\Delta C_l \approx -\lambda_p\left((T_c - T_s)\Delta f + f\Delta T_c\right)$ is also mostly due to the reductions in f (fig. 3 b, right bracket). Finally, almost the entire increase in the 150 km-domain clear-sky longwave cooling can be explained by their cloud-layer drying, in line with Fildier et al. (2023)'s theory. That is, given the domain-averaged I, $-\Delta F^{\uparrow}_{l,c} \approx -\partial F^{\uparrow}_{l,c}/\partial I \times \Delta I$, as estimated by linear regression (fig. 3 b, central bracket). This result echoes how mean drying in the presence of aggregated deep convection allows the clear skies of such domains to radiate more efficiently to space than in disaggregated situations (e.g. Bretherton et al., 2005; Bony et al., 2020), though the simulated shallow convective difference is weaker.

4 Mesoscale self-organisation weakly modifies a small trade cumulus feedback

In all, self-organisation in 150 km domains gives a small, systematic cooling compared to 10 km domains, from reductions in f, increases in α_c and reductions in I. Yet, the resultant modifications of the radiation budget's two components that are most sensitive to domain size, $F^{\uparrow}_{l,c}$ and C_s, usually remain weak compared to variability in $F^{\uparrow}_{l,c}$ and C_s associated with changes in the imposed CCFs $x = [\theta_{l_s}, U, \Gamma_{\theta_l}, h_{q_t}, w_{ls}]$. To show this, we compute the sensitivities $\partial_{x_i} F^{\uparrow}_{l,c}$ and $\partial_{x_i} C_s$ (we denote partial differentiation Y to x_i as $\partial_{x_i} Y$). We calculate $\partial_{x_i} C_s$ and $\partial_{x_i} F^{\uparrow}_{l,c}$ by averaging C_s and $F^{\uparrow}_{l,c}$ over 30-54 h, and linearly regressing them on sweeps in each CCF x_i, keeping other CCFs constant at their central value. We then multiply the sensitivities by x_i's varied range, giving variability in C_s and $F^{\uparrow}_{l,c}$ due to climatologically representative variations in x_i.

Fig. 3 c shows the familiar, strong cooling response of $F^{\uparrow}_{l,c}$ to warming the entire tropical atmosphere by a roughly constant amount (θ_{l_s}, i.e. the Planck response) and increasing Γ_{θ_l} (the lapse rate response), and the warming response to increasing q_t (the water vapour response). The latter is measured both directly (by increasing h_{q_t}) and indirectly, by i) raising U, which boosts the surface moisture fluxes, moistening the boundary layer, and ii) making w_{ls} more positive, which reduces the vertical advective drying of large-scale subsidence (see fig. S3). The largest three sensitivities are an order of magnitude larger than differences between large and small domains. That is, the response of clear-sky radiation to changes in variables that also will change with tropical warming (θ_{l_s}, Γ_{θ_l}, h_{q_t}), is insensitive to whether shallow convection is self-organised at mesoscales or not.

The sensitivities $\partial_{x_i} C_s$ (fig. 3 d) are also generally larger than differences between large and small domains, although C_s in large domains is structurally less sensitive to changes in U, and more sensitive to changes in h_{q_t} and w_{ls}. Yet, focusing on $\partial_{\theta_{l_s}} C_s$ and $\partial_{\Gamma_{\theta_l}} C_s$, the largest two contributors to observed variability in trade cumulus C_s (Scott et al., 2020) and its response to warming (Myers et al., 2021), both large and small domains agree that they are near-zero.

The predicted $\partial_{\theta_{l_s}} C_s$ (0.07 Wm^{-2} K^{-1} and 0.11 Wm^{-2} K^{-1} for large and small domains respectively) also align with satellite observations over the North-Atlantic trades (0.11-0.13 Wm^{-2} K^{-1}, Scott et al., 2020; Cesana & Del Genio, 2021), as do the simulated reductions in f (1% K^{-1}, against 1-2% K^{-1} in Mieslinger et al., 2019; Cesana et al., 2019). Contrarily, the simulated $\partial_{\Gamma_{\theta_l}} C_s$ (-0.48 and 0.65 Wm^{-2} for large and small domains) are an order of magnitude smaller than Scott et al. (2020)'s sensitivity of satellite-derived radiative fluxes to reanalysis-inferred Estimated Inversion Strength (EIS, Wood & Bretherton, 2006): -5.44 Wm^{-2} over the EIS range implied by our Γ_{θ_l} sweep. In the simulations, the smaller $\partial_{\Gamma_{\theta_l}} C_s$ arises from offsetting effects: Stabilising the free troposphere lowers and strengthens the trade inversion (e.g. Bellon & Stevens, 2012, fig. S4 c, h), reducing the shallow convection's depth and α_c, but increasing inversion cloudiness and f (fig. S5 c, h). Scott et al. (2020) suggest that raising the EIS in trade-cumulus regimes increases both f *and* α_c, likely because they do not find that increasing EIS reduces cloud-top height (their fig. S11 b). This places the observations in conflict with bulk theory and our simulations. Since Scott et al. (2020) identify EIS as the second strongest control on C_s in trade-cumulus regions, resolving this inconsistency is warranted.

The fact that mesoscale self-organisation only weakly modifies $\partial_{x_i} F^{\uparrow}_{l,c}$ and $\partial_{x_i} C_s$, explains why both small-domain LESs and CCF-observation frameworks project the same weak trade cumulus feedback $\lambda_t = \partial_{x_i} C_s \times \partial_{T_s} x_i$: Since $\partial_{x_i} C_s$ are similar to what is observed in both our large- and small-domain LESs, were we to multiply them with sensitivities of x_i to surface warming ($\partial_{T_s} x_i$) from climate models under a scenario of climate change, our large- and small-domain ensembles would project similar, small estimates of the trade-cumulus feedback as studies that take this approach based on the observed $\partial_{x_i} C_s$ (Myers et al., 2021; Cesana & Del Genio, 2021; Ceppi & Nowack, 2021) (though there would be slightly less cooling from the smaller sensitivity to Γ_{θ_l}).

5 A symmetry hypothesis for mesoscale cloud-circulation coupling

In essence, our results suggest that self-generated mesoscale circulations, be they through moisture-convection feedbacks or cold pool dynamics, do not greatly modify the mean C_s in fields of shallow cumuli. This is perhaps somewhat surprising, given strong observed correlations between mesoscale vertical motion and cloudiness in the trades (George et al., 2021; Vogel et al., 2022). Such correlations are present in our ensemble too: The 10×10 km^2-averaged f (f_{10}) rises almost proportionally with 10×10 km^2-averaged w evaluated at 1000 m (w_{10}) (fig. 4 a-b). Yet, because mesoscale variability in active cloudiness *generates* w_{10} (Janssens et al., 2024), ascending sub-domains with large (convective) cloudiness must be compensated by descending sub-domains with low cloudiness, for the circulations to exist at all. In our simulations, these opposing effects almost cancel: Expressing the w_{10}-bin averaged f_{10} (red line, fig. 4 b) as

$$f_{10}(w_{10}) = f_c + f'_{10}(w_{10}), \tag{2}$$

where f_c is the (w_{10}-independent) 10-km domain simulation f, then the contribution to f from mesoscale cloud-circulation coupling ($f'_{10}(w_{10})$, weighted by the marginal probability density function of w_{10}, $p(w_{10})$) is near-zero, i.e.

$$f = f_c + \int_{-\infty}^{\infty} p(w_{10}) f'_{10}(w_{10}) dw_{10} \approx f_c. \tag{3}$$

So, in these simulations, mesoscale circulations give large, skewed variability in 10 km-f across a domain at any time (fig. 4 a), but small changes in 150 km-f relative to this variability, both in a given simulation (fig. 4 b) and across the ensemble (fig. 4 c). That is, the ascending and descending branches of mesoscale circulations are *nearly symmetric* in their opposing effect on f, and C_s (note that $f'_{10}(w)$ does not need to be linear for eq. 3 to hold, see e.g. $w_{10} < 0$ sub-domains in fig. 4 b where both cloud anvils flowing from convecting regions and cloud-free sub-domains with strong compensating subsidence pull $f'_{10}(w_{10})$ away from linearity).

Such symmetry may be exaggerated in our doubly periodic LES, where w must vanish at the domain scale. Yet also in nature, once the coherent vertical motion of the large-scale tropical circulation is subtracted, there is no *a priori* reason to expect entire trade-wind regimes to exhibit a mean vertical cloud-layer velocity. Hence, the symmetry in our simulations emphasises that circulations of scales smaller than the entire trades can only modify C_s if their ascending branches asymmetrically affect f or α_c with respect to their descending branches. Across our ensemble, these effects are small ($\sim 2\%$) relative to their imprint on mesoscale variability ($\sim 20\%$, fig. 4 c), and buffered by both the opposite-sign responses of f or α_c (fig. 2 f-g) and the increased longwave cooling (fig. 3 b), giv-

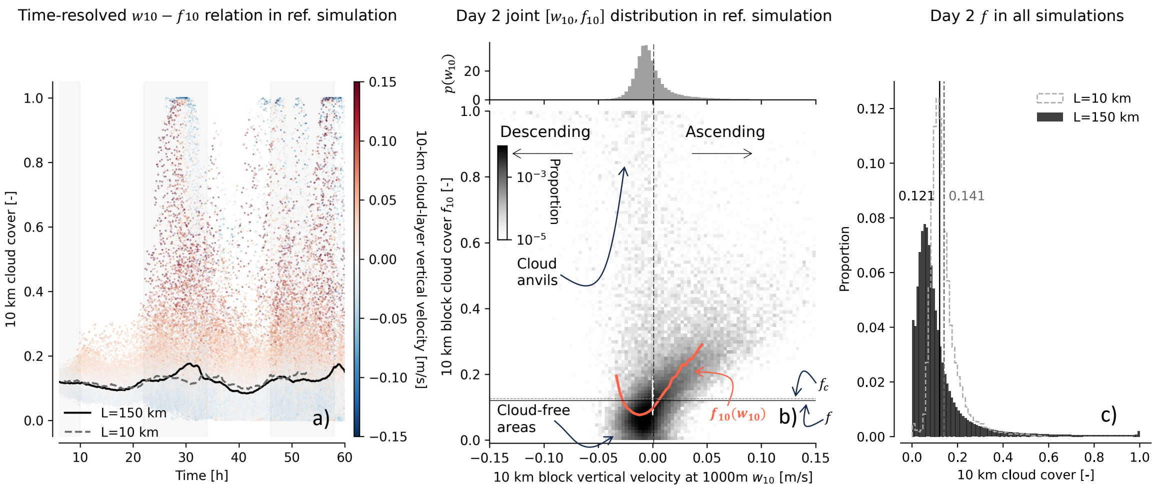

Figure 4. a) Time-evolution of cloud cover f_{10} (y-axis) and cloud-layer (1000 m) vertical motion w_{10} (colours) averaged over 10 km × 10 km sub-domains in the Cloud Botany reference simulation, with the 150 km and 10 km domain-average f (lines). b) Joint histogram of w_{10} and f_{10} and marginal density function $p(w_{10})$ in reference simulation between 30-54 h (day 2, shading as fig. 2), with white scatter indicating 10 km-domain f at $w_{10} = 0$, horizontal lines indicating 150 km- and 10km-domain f (f, f_c), and the red line indicating f_{10} averaged over a w-bin, $f_{10}(w_{10})$. c) Histogram of day 2-f in all simulations of the 150 km ensemble (black) and 10 km ensemble (grey outline). Vertical lines mark the mean f across both ensembles.

ing changes in TOA net radiation (-0.5 W m^{-2}) which are small relative to variability induced by larger-scale cloud-controlling factors (fig. 3 c-d).

Of course, this discussion hinges on the realism of idealised LESs, which retain several biases. The ensemble-averaged f (0.12) is substantially lower than the EUREC^{4}A average (0.42, Mieslinger et al., 2022). The relative importance of C_l (ensemble-average 1.1 W m^{-2}) to C_s (-7.2 W m^{-2}) is likely underestimated (Schulz & Stevens, 2023). Our environmental control factors are simpler and sparser than in nature. The simulated mesoscale dynamics are sensitive to arbitrary model choices (Li et al., 2015; Janssens et al., 2023); simulations at half (50 m) the horizontal grid spacing in four ensemble members produce slightly more clouds and 15% larger C_s, though their organisation develops at a similar time scale at finer resolution. Finally, our doubly periodic 150 km domains are too small and idealised to simulate mesoscale cloud structures and circulations which in nature grow from pre-existing disturbances, up to scales of 700 km (Janssens et al., 2024). What these LESs do instead, is pose the hypothesis that mesoscale circulations are symmetric in their effects on the TOA radiation balance, and thus will not substantially alter contemporary estimates of a weak trade cumulus contribution to the cloud feedback on warming. We now require observations akin to fig. 4 b to truly understand whether the intrinsic tendency of trade cumuli to self-organise is just beautiful and striking, or whether it impacts global climate.

6 Open Research

The 150 km and 10 km Cloud Botany simulations are hosted at the German Climate Computing Center (DKRZ) and are freely available through the EUREC^{4}A intake catalog (`https://howto.eurec4a.eu/botany_dales.html`). The metrics underlying fig. 1 have been computed with the Cloudmetrics code package (Denby & Janssens, 2022). These metrics, and all code required to produce the figures and data herein are available from `https://doi.org/10.5281/zenodo.8089287` (Janssens, 2024). Finally, the meteorological cloud-radiative kernels computed by Scott et al. (2020) have been retrieved from `https://github.com/tamyers87/meteorological_cloud_radiative_kernels`. We thank these authors for making their data publicly available.

Acknowledgments
MJ thanks Jordi Vilà and Raphaela Vogel for fruitful feedback on an earlier version of this manuscript. APS and FJ acknowledge support from the European Union's Horizon 2020 research and innovation program under grant agreement no. 820829 (CONSTRAIN project). FG and PA acknowledge support from The Branco Weiss Fellowship - Society in Science, administered by ETH Zürich. FG further acknowledges funding by the European Union (ERC, MesoClou, 101117462). Views and opinions expressed are however those of the author(s) only and do not necessarily reflect those of the European Union or the European Research Council Executive Agency. Neither the European Union nor the granting authority can be held responsible for them. This research used computational resources of Fugaku provided by RIKEN through the HPCI System Research Project (Project ID: hp200321), and the Dutch National Supercomputer Snellius, administered by SURF. We also thank DKRZ for hosting the Cloud Botany data set under project ID bm1349.

References

Albrecht, B. A. (1993). Effects of precipitation on the thermodynamic structure of the trade wind boundary layer. *Journal of Geophysical Research: Atmospheres*, *98*(D4), 7327–7337.

Alinaghi, P., Janssens, M., Choudhury, G., Goren, T., Siebesma, A. P., & Glassmeier, F. (2023). Shallow cumulus cloud fields are optically thicker when they are more clustered. *Quarterly Journal of the Royal Meteorological Society*.

Alinaghi, P., Siebesma, P., Jansson, F., Janssens, M., & Glassmeier, F. (2024). External drivers and mesoscale self-organization of shallow cold pools in the trade-wind regime. *Authorea Preprints*.

Bellon, G., & Stevens, B. (2012). Using the sensitivity of large-eddy simulations to evaluate atmospheric boundary layer models. *Journal of the Atmospheric Sciences*, *69*(5), 1582–1601.

Benner, T. C., & Curry, J. A. (1998). Characteristics of small tropical cumulus clouds and their impact on the environment. *Journal of Geophysical Research: Atmospheres*, *103*(D22), 28753–28767.

Blossey, P. N., Bretherton, C. S., Zhang, M., Cheng, A., Endo, S., Heus, T., … Xu, K.-M. (2013). Marine low cloud sensitivity to an idealized climate change: The CGILS LES intercomparison. *Journal of Advances in Modeling Earth Systems*, *5*(2), 234–258.

Bony, S., & Dufresne, J.-L. (2005). Marine boundary layer clouds at the heart of tropical cloud feedback uncertainties in climate models. *Geophysical Research Letters*, *32*(20).

Bony, S., Semie, A., Kramer, R. J., Soden, B., Tompkins, A. M., & Emanuel, K. A. (2020). Observed modulation of the tropical radiation budget by deep convective organization and lower-tropospheric stability. *AGU Advances*, *1*(3), e2019AV000155.

Bretherton, C. S., McCaa, J. R., & Grenier, H. (2004). A new parameterization for shallow cumulus convection and its application to marine subtropical cloud-topped boundary layers. Part I: Description and 1D results. *Monthly Weather Review*, *132*(4), 864–882.

Bretherton, C. S., Blossey, P. N., & Khairoutdinov, M. (2005). An energy-balance analysis of deep convective self-aggregation above uniform SST. *Journal of the Atmospheric Sciences*, *62*(12), 4273–4292.

Bretherton, C. S., Blossey, P. N., & Jones, C. R. (2013). Mechanisms of marine low cloud sensitivity to idealized climate perturbations: A single-LES exploration extending the CGILS cases. *Journal of Advances in Modeling Earth Systems*, *5*(2), 316–337.

Bretherton, C. S. (2015). Insights into low-latitude cloud feedbacks from high-resolution models. *Philosophical Transactions of the Royal Society A: Mathematical, Physical and Engineering Sciences*, *373*(2054), 20140415.

Bretherton, C. S., & Blossey, P. N. (2017). Understanding mesoscale aggregation of shallow cumulus convection using large-eddy simulation. *Journal of Advances in Modeling Earth Systems*, *9*(8), 2798–2821.

Brueck, M., Nuijens, L., & Stevens, B. (2015). On the seasonal and synoptic time-scale variability of the North Atlantic trade wind region and its low-level clouds. *Journal of the Atmospheric Sciences*, *72*(4), 1428–1446.

Ceppi, P., & Nowack, P. (2021). Observational evidence that cloud feedback amplifies global warming. *Proceedings of the National Academy of Sciences*, *118*(30), e2026290118.

Cesana, G., Del Genio, A. D., Ackerman, A. S., Kelley, M., Elsaesser, G., Fridlind, A. M., ... Yao, M.-S. (2019). Evaluating models' response of tropical low clouds to sst forcings using calipso observations. *Atmospheric Chemistry and Physics*, *19*(5), 2813–2832.

Cesana, G., & Del Genio, A. D. (2021). Observational constraint on cloud feedbacks suggests moderate climate sensitivity. *Nature Climate Change*, *11*(3), 213–218.

Coakley, J. A., & Chylek, P. (1975). The two-stream approximation in radiative transfer: Including the angle of the incident radiation. *Journal of Atmospheric Sciences*, *32*(2), 409–418.

Dauhut, T., Couvreux, F., Bouniol, D., Beucher, F., Volkmer, L., Pörtge, V., ... others (2023). Flower trade-wind clouds are shallow mesoscale convective systems. *Quarterly Journal of the Royal Meteorological Society*, *149*(750), 325–347.

Denby, L., & Janssens, M. (2022). *cloudsci/cloudmetrics.* Zenodo. doi: 10.5281/zenodo.7506966

Feingold, G., Balsells, J., Glassmeier, F., Yamaguchi, T., Kazil, J., & McComiskey, A. (2017). Analysis of albedo versus cloud fraction relationships in liquid water clouds using heuristic models and large eddy simulation. *Journal of Geophysical Research: Atmospheres*, *122*(13), 7086–7102.

Fildier, B., Muller, C., Pincus, R., & Fueglistaler, S. (2023). How moisture shapes low-level radiative cooling in subsidence regimes. *AGU Advances*. doi: https://doi.org/10.1029/2023AV000880

George, G., Stevens, B., Bony, S., Klingebiel, M., & Vogel, R. (2021). Observed impact of mesoscale vertical motion on cloudiness. *Journal of the Atmospheric Sciences*, *78*(8), 2413–2427.

George, G., Stevens, B., Bony, S., Vogel, R., & Naumann, A. K. (2023). Widespread shallow mesoscale circulations observed in the trades. *Nature Geoscience*. doi: 10.1038/s41561-023-01215-1

Iacono, M. J., Delamere, J. S., Mlawer, E. J., Shephard, M. W., Clough, S. A., & Collins, W. D. (2008). Radiative forcing by long-lived greenhouse gases: Calculations with the AER radiative transfer models. *Journal of Geophysical Research: Atmospheres*, *113*(D13).

Janssens, M. (2024, August). *Supporting data for manuscript "Symmetry in mesoscale circulations explains weak impact of trade cumulus self-organisation on the radiation budget in large-eddy simulations"* [Dataset and software].

Zenodo. Retrieved from https://doi.org/10.5281/zenodo.13619668 doi: 10.5281/zenodo.13619668

Janssens, M., George, G., Schulz, H., Couvreux, F., & Bouniol, D. (2024). Shallow convective heating in weak temperature gradient balance explains mesoscale vertical motions in the trades. *ESS Open Archive*. doi: 10.22541/essoar.171415887.72921250/v1

Janssens, M., Vilà-Guerau De Arellano, J., Scheffer, M., Antonissen, C., Siebesma, A. P., & Glassmeier, F. (2021). Cloud patterns in the trades have four interpretable dimensions. *Geophysical Research Letters*, *48*(5), e2020GL091001.

Janssens, M., Vilà-Guerau-De Arellano, J., Van Heerwaarden, C. C., De Roode, S. R., Siebesma, A. P., & Glassmeier, F. (2022). Nonprecipitating shallow cumulus convection is intrinsically unstable to length scale growth. *Journal of the Atmospheric Sciences*, *80*(3), 849–870.

Janssens, M., Vilà-Guerau De Arellano, J., Van Heerwaarden, C. C., Van Stratum, B. J., De Roode, S. R., Siebesma, A. P., & Glassmeier, F. (2023). The time scale of shallow convective self-aggregation in large-eddy simulations is sensitive to numerics. *Journal of Advances in Modeling Earth Systems*, *15*(1), e2022MS003292.

Jansson, F., Janssens, M., Grönqvist, J. H., Siebesma, P., Glassmeier, F., Attema, J. J., … others (2023). Cloud botany: Shallow cumulus clouds in an ensemble of idealized large-domain large-eddy simulations of the trades. *Journal of Advances in Modeling Earth Systems*, *10*, e2023MS003796.

Klein, S. A., Hall, A., Norris, J. R., & Pincus, R. (2017). Low-cloud feedbacks from cloud-controlling factors: a review. In R. Pincus, M. Winker, S. Bony, & B. Stevens (Eds.), *Shallow clouds, water vapor, circulation, and climate sensitivity* (pp. 135–157). Springer.

Lamaakel, O., & Matheou, G. (2022). Organization development in precipitating shallow cumulus convection: Evolution of turbulence characteristics. *Journal of the Atmospheric Sciences*, *79*(9), 2419–2433.

Li, Z., Zuidema, P., Zhu, P., & Morrison, H. (2015). The sensitivity of simulated shallow cumulus convection and cold pools to microphysics. *Journal of the Atmospheric Sciences*, *72*(9), 3340–3355.

McKim, B., Bony, S., & Dufresne, J.-L. (2024). Weak anvil cloud area feedback suggested by physical and observational constraints. *Nature Geoscience*, 1–6.

Mieslinger, T., Horváth, Á., Buehler, S. A., & Sakradzija, M. (2019). The dependence of shallow cumulus macrophysical properties on large-scale meteorology as observed in ASTER imagery. *Journal of Geophysical Research: Atmospheres*, *124*(21), 11477–11505.

Mieslinger, T., Stevens, B., Kölling, T., Brath, M., Wirth, M., & Buehler, S. A. (2022). Optically thin clouds in the trades. *Atmospheric Chemistry and Physics*, *22*(10), 6879–6898.

Myers, T. A., & Norris, J. R. (2016). Reducing the uncertainty in subtropical cloud feedback. *Geophysical Research Letters*, *43*(5), 2144–2148.

Myers, T. A., Scott, R. C., Zelinka, M. D., Klein, S. A., Norris, J. R., & Caldwell, P. M. (2021). Observational constraints on low cloud feedback reduce uncertainty of climate sensitivity. *Nature Climate Change*, *11*(6), 501–507.

Narenpitak, P., Kazil, J., Yamaguchi, T., Quinn, P. K., & Feingold, G. (2021). From sugar to flowers: A transition of shallow cumulus organization during ATOMIC. *Journal of Advances in Modeling Earth Systems*, *13*, e2021MS002619.

Nuijens, L., Stevens, B., & Siebesma, A. P. (2009). The environment of precipitating shallow cumulus convection. *Journal of the Atmospheric Sciences*, *66*(7), 1962–1979.

O, K.-T., Wood, R., Tseng, H., et al. (2018). Deeper, precipitating PBLs associated with optically thin veil clouds in the Sc-Cu transition. *Geophysical Re-*

search Letters, *45*(10), 5177–5184.
Plank, V. G. (1969). The size distribution of cumulus clouds in representative Florida populations. *Journal of Applied Meteorology and Climatology*, *8*(1), 46–67.
Radtke, J., Mauritsen, T., & Hohenegger, C. (2021). Shallow cumulus cloud feedback in large eddy simulations–bridging the gap to storm-resolving models. *Atmospheric Chemistry and Physics*, *21*(5), 3275–3288.
Radtke, J., Vogel, R., Ament, F., & Naumann, A. K. (2023). Spatial organisation affects the pathway to precipitation in simulated trade-wind convection. *Authorea*. doi: https://doi.org/10.22541/essoar.167979635.58663858/v1
Schulz, H., & Stevens, B. (2023). On the representation of shallow convection in the trades by large-domain, hecto-meter, large-eddy simulations. *EarthArXiv*. doi: https://doi.org/10.31223/X5H651
Scott, R. C., Myers, T. A., Norris, J. R., Zelinka, M. D., Klein, S. A., Sun, M., & Doelling, D. R. (2020). Observed sensitivity of low-cloud radiative effects to meteorological perturbations over the global oceans. *Journal of Climate*, *33*(18), 7717–7734.
Seifert, A., & Heus, T. (2013). Large-eddy simulation of organized precipitating trade wind cumulus clouds. *Atmosperic Chemistry and Physics*, *13*(11), 5631–5645.
Sherwood, S. C., Webb, M. J., Annan, J. D., Armour, K. C., Forster, P. M., Hargreaves, J. C., ... others (2020). An assessment of Earth's climate sensitivity using multiple lines of evidence. *Reviews of Geophysics*, *58*(4), e2019RG000678.
Stephens, G. L. (1978). Radiation profiles in extended water clouds. II: Parameterization schemes. *Journal of Atmospheric Sciences*, *35*(11), 2123–2132.
Stevens, B., & Seifert, A. (2008). Understanding macrophysical outcomes of microphysical choices in simulations of shallow cumulus convection. *Journal of the Meteorological Society of Japan. Ser. II*, *86*, 143–162.
Tan, Z., Schneider, T., Teixeira, J., & Pressel, K. G. (2017). Large-eddy simulation of subtropical cloud-topped boundary layers: 2. Cloud response to climate change. *Journal of Advances in Modeling Earth Systems*, *9*(1), 19–38.
Vial, J., Dufresne, J.-L., & Bony, S. (2013). On the interpretation of inter-model spread in CMIP5 climate sensitivity estimates. *Climate Dynamics*, *41*(11-12), 3339–3362.
Vial, J., Vogel, R., & Schulz, H. (2021). On the daily cycle of mesoscale cloud organization in the winter trades. *Quarterly Journal of the Royal Meteorological Society*, *147*(738), 2850–2873.
Vial, J., Albright, A. L., Vogel, R., Musat, I., & Bony, S. (2023). Cloud transition across the daily cycle illuminates model responses of trade cumuli to warming. *Proceedings of the National Academy of Sciences*, *120*(8), e2209805120.
Vogel, R., Nuijens, L., & Stevens, B. (2016). The role of precipitation and spatial organization in the response of trade-wind clouds to warming. *Journal of Advances in Modeling Earth Systems*, *8*(2), 843–862.
Vogel, R., Nuijens, L., & Stevens, B. (2019). Influence of deepening and mesoscale organization of shallow convection on stratiform cloudiness in the downstream trades. *Quarterly Journal of the Royal Meteorological Society*.
Vogel, R., Albright, A. L., Vial, J., George, G., Stevens, B., & Bony, S. (2022). Strong cloud–circulation coupling explains weak trade cumulus feedback. *Nature*, *612*, 696-–700.
Wood, R., & Bretherton, C. S. (2006). On the relationship between stratiform low cloud cover and lower-tropospheric stability. *Journal of Climate*, *19*(24), 6425–6432.
Wood, R., O, K.-T., Bretherton, C. S., Mohrmann, J., Albrecht, B. A., Zuidema, P., ... others (2018). Ultraclean layers and optically thin clouds in the

stratocumulus-to-cumulus transition. Part I: Observations. *Journal of the Atmospheric Sciences*, *75*(5), 1631–1652.

Zelinka, M. D., Myers, T. A., McCoy, D. T., Po-Chedley, S., Caldwell, P. M., Ceppi, P., … Taylor, K. E. (2020). Causes of higher climate sensitivity in CMIP6 models. *Geophysical Research Letters*, *47*(1), e2019GL085782.

Zhao, G., & Di Girolamo, L. (2007). Statistics on the macrophysical properties of trade wind cumuli over the tropical western Atlantic. *Journal of Geophysical Research: Atmospheres*, *112*(D10).

Supporting Information for “Symmetry in mesoscale circulations explains weak impact of trade cumulus self-organisation on the radiation budget in large-eddy simulations”

M. Janssens[1,2], F. Jansson[2], P. Alinaghi[2], F. Glassmeier[2], A. P. Siebesma[2,3]

[1]Wageningen University & Research, Wageningen, The Netherlands

[2]Delft University of Technology, Delft, The Netherlands

[3]Royal Netherlands Meteorological Institute, De Bilt, The Netherlands

Contents of this file

1. Text S1
2. Figures S1 to S5

Text S1.

The profile $\alpha_c(z)$ in the main text's Figure 2 g is constructed in the zenith-angle Θ-corrected plane-parallel approximation (e.g. Feingold et al., 2017):

$$\alpha_c \approx \frac{\tau_c}{\tau_c + \frac{2\cos\Theta}{1-g}} \tag{1}$$

We take the asymmetry parameter $g = 0.85$, and compute cloud-optical depth τ_c in each cloudy column before averaging, assuming the clouds are adiabatic (Stephens, 1978):

$$\tau_c = 0.19\mathcal{L}^{\frac{5}{6}}N^{\frac{1}{3}} \tag{2}$$

In this relation, $\mathcal{L}$ is the liquid-water path, and $N = 70\text{cm}^{-3}$ the fixed droplet number concentration in our simulations. α_c can in this scenario only vary due to changes in the clouds' liquid water content at a height z, or changes in their geometrical thickness. To decompose the two contributions, Figure 2 g) plots $\alpha_c(z)$, the cumulative contribution of all model levels below z towards the cloud-albedo α_c.

Since large domains support more horizontally extensive clouds than small domains (larger L_c in Figure 1, Figure S2), and large cumuli are known to be both geometrically thicker and more adiabatic (Plank, 1969; Benner & Curry, 1998; Zhao & Di Girolamo, 2007; Feingold et al., 2017), the large-domain clouds have a higher $\mathcal{L}$, as shown in Figure 2 g).

References

Benner, T. C., & Curry, J. A. (1998). Characteristics of small tropical cumulus clouds and their impact on the environment. *Journal of Geophysical Research: Atmospheres*, *103*(D22), 28753–28767.

Feingold, G., Balsells, J., Glassmeier, F., Yamaguchi, T., Kazil, J., & McComiskey, A. (2017). Analysis of albedo versus cloud fraction relationships in liquid water clouds using heuristic models and large eddy simulation. *Journal of Geophysical Research: Atmospheres*, *122*(13), 7086–7102.

Janssens, M., Vilà-Guerau De Arellano, J., Scheffer, M., Antonissen, C., Siebesma, A. P., & Glassmeier, F. (2021). Cloud patterns in the trades have four interpretable dimensions. *Geophysical Research Letters*, *48*(5), e2020GL091001.

Plank, V. G. (1969). The size distribution of cumulus clouds in representative Florida populations. *Journal of Applied Meteorology and Climatology*, *8*(1), 46–67.

Stephens, G. L. (1978). Radiation profiles in extended water clouds. II: Parameterization schemes. *Journal of Atmospheric Sciences*, *35*(11), 2123–2132.

Zhao, G., & Di Girolamo, L. (2007). Statistics on the macrophysical properties of trade wind cumuli over the tropical western Atlantic. *Journal of Geophysical Research: Atmospheres*, *112*(D10).

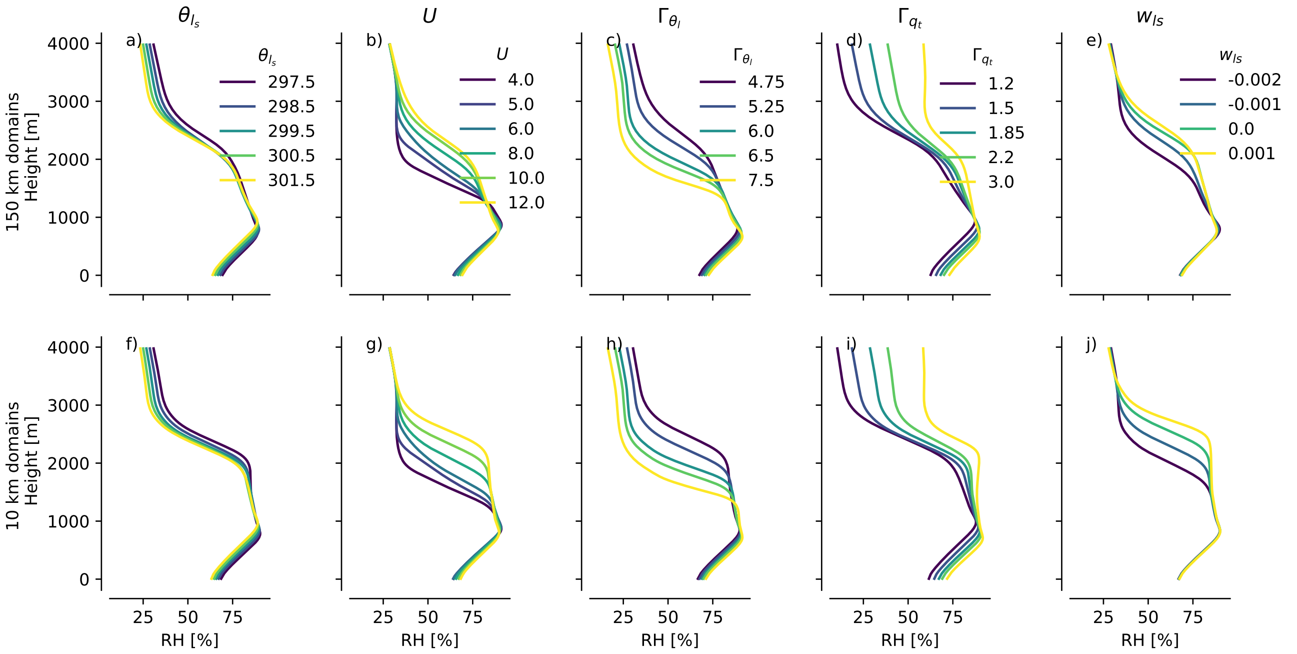

Figure S1. Variation in relative humidity with $x_i \in \left[\theta_{l_s}, U, \Gamma_{\theta_{l_s}}, \Gamma_{q_t}, w_{ls}\right]$ (columns) in simulations corresponding to those plotted in the main text's fig. 3, in 150 km domains (top row) and 10 km domains (bottom row), averaged over daytime on day 2 of simulation. Colours indicate the imposed changes in x_i.

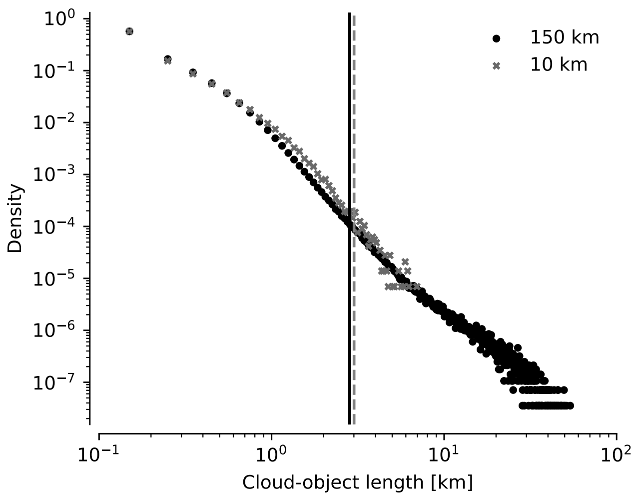

Figure S2. Cloud-object size distribution, averaged over all simulations and 30-54 hr, in 150 km domains (black circles) and 10 km domains (grey crosses). Vertical lines indicate the means of the distributions, $\bar{l}$ as also included in the main text's fig. 1, computed by identifying cloud objects following Janssens et al. (2021) and binning over 100 m sized bins.

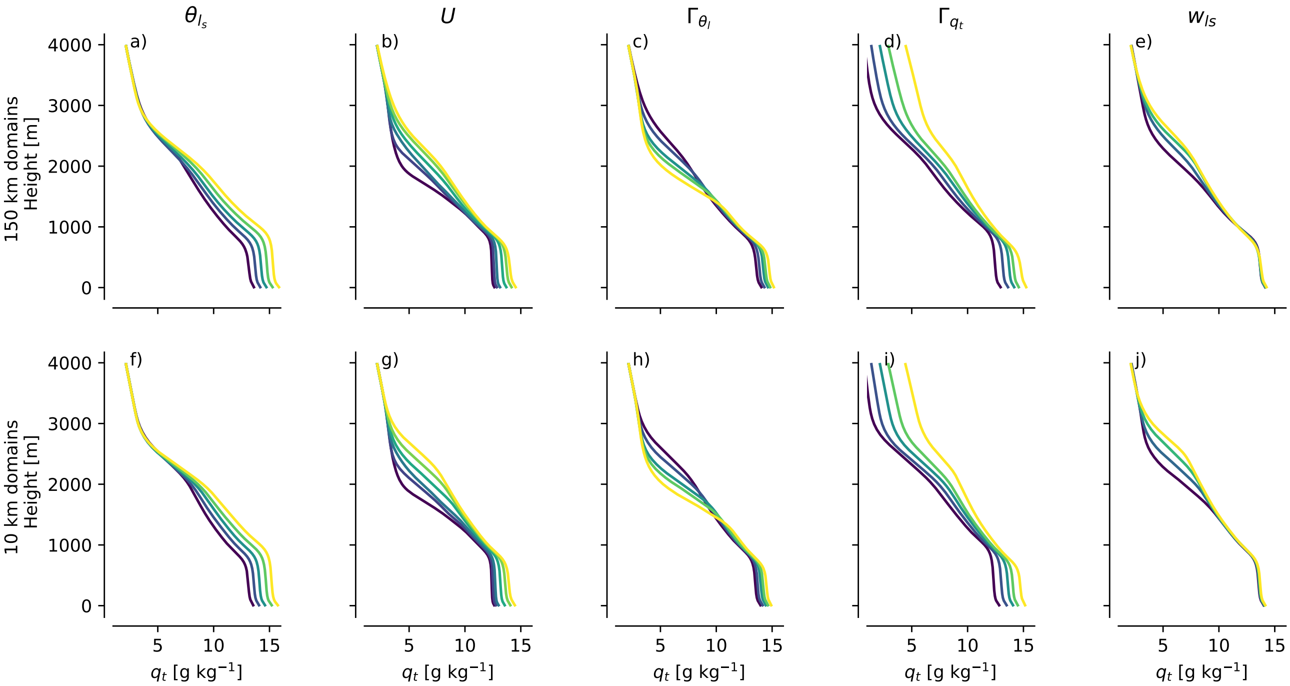

Figure S3. As fig. S1, for horizontally averaged total water specific humidity, q_t.

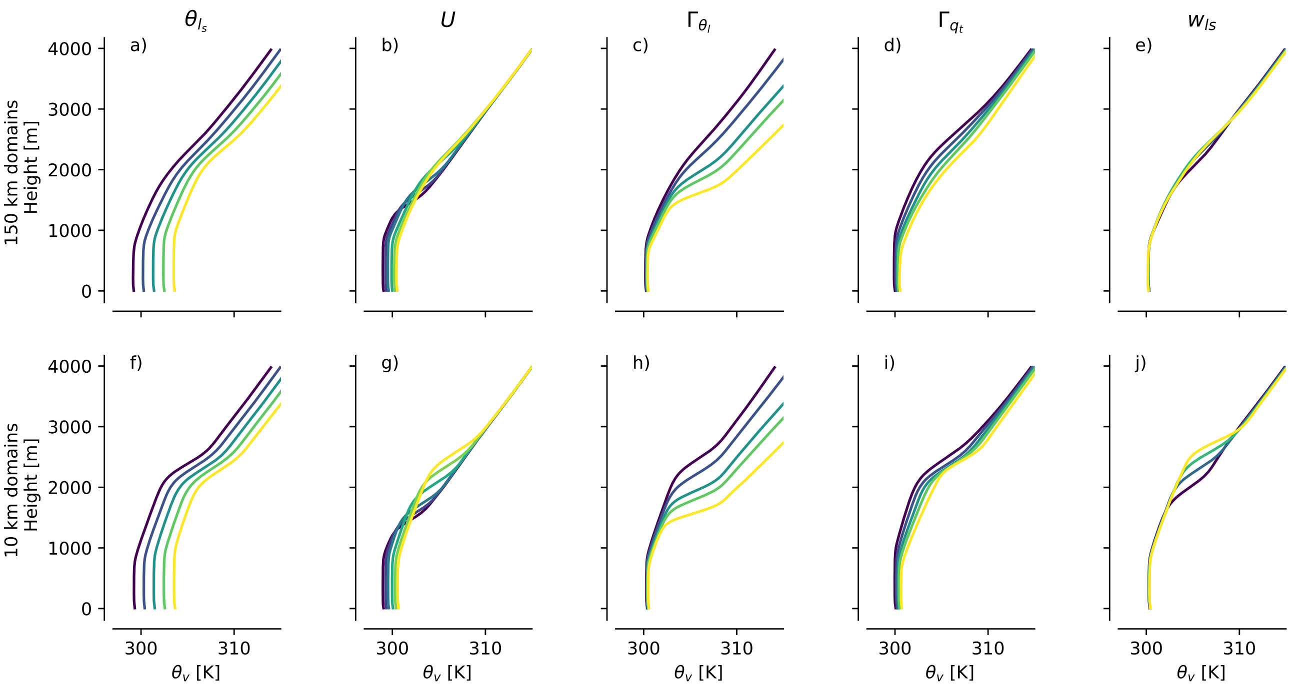

Figure S4. As fig. S1, for horizontally averaged virtual potential temperature, θ_v.

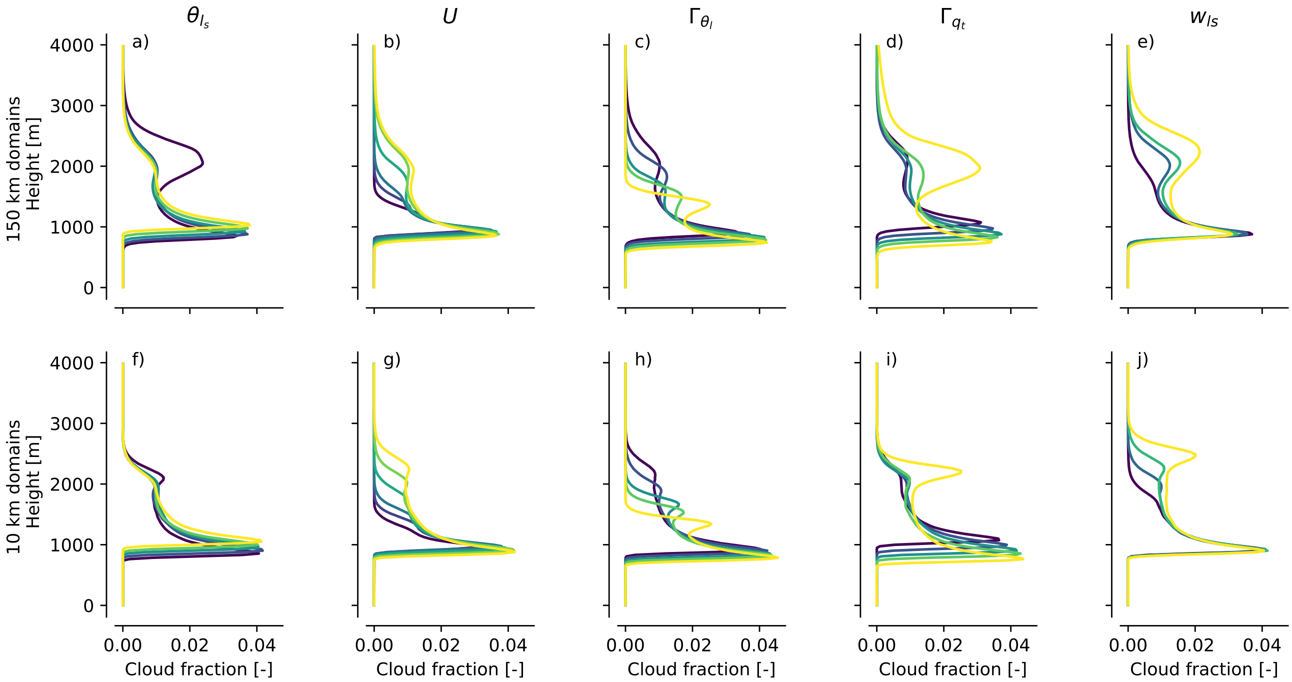

Figure S5. As fig. S1, for height-wise cloud fraction.